



## Contents

<b>1. Tasks</b>	<b>3</b>
<b>2. Theoretical basics</b>	<b>4</b>
2.1. Atomic models . . . . .	4
2.1.1. Drop model . . . . .	4
2.1.2. Fermi-gas-model . . . . .	5
2.2. Shell model . . . . .	5
2.3. Radioactive decay . . . . .	5
2.4. $\alpha$ -decay . . . . .	6
2.5. $\beta$ -decay . . . . .	6
2.6. $\gamma$ -decay . . . . .	7
2.7. Inner conversion . . . . .	7
2.8. Interaction of electromagnetic radiation with matter . . . . .	7
2.8.1. Photo effect . . . . .	8
2.8.2. Compton effect . . . . .	8
2.8.3. Pair coupling . . . . .	8
2.9. Used radioactive samples . . . . .	9
2.9.1. $^{22}\text{Na}$ . . . . .	9
2.9.2. $^{60}\text{Co}$ . . . . .	9
2.9.3. $^{152}\text{Eu}$ . . . . .	9
2.9.4. $^{228}\text{Th}$ . . . . .	10
2.10. Devices . . . . .	10
2.10.1. Inorganic scintillators . . . . .	10
2.10.2. Organic scintillators . . . . .	11
2.10.3. Photo multiplier . . . . .	11
2.10.4. Pre- and main-amplifier (PA/MA) . . . . .	12
2.10.5. Single and multi channel analyzer (SCA/MCA) . . . . .	12
<b>3. Setup and procedure</b>	<b>13</b>
<b>4. Data analysis</b>	<b>15</b>
4.1. Preparation . . . . .	15
4.2. Background measurement . . . . .	17
4.3. Characterisation of the MCA . . . . .	18
4.4. Energy spectrum of the $^{228}\text{Th}$ decay . . . . .	23
4.5. Angle distribution of the $^{22}\text{N}$ annihilation photons . . . . .	27
<b>5. Summary and discussion</b>	<b>29</b>
<b>A. List of Figures</b>	<b>30</b>
<b>B. List of Tables</b>	<b>30</b>
<b>C. References</b>	<b>31</b>
<b>D. Appendix</b>	<b>32</b>
D.1. Additional plots . . . . .	32
D.2. Original data . . . . .	33

## 1. Tasks

In this experiment there are two main tasks. The first part starts with measuring the spectra of isotopes of europium, cobalt and sodium for about half an hour. These measurements are necessary in order to be able to compare the channels in which the data gets measured to their energy. Furthermore the spectrum of thorium has to be measured over night and the background for tree hours.

In the second part, the angle distribution of annihilation photons of sodium is to be measured.

In this protocol we used the package *mhchem*, not *isotope* as proposed by [2], since that package isn't up to date and doesn't work properly.

## 2. Theoretical basics

### 2.1. Atomic models

It is not possible to give one model of atomic cores, that describes their behaviour in all aspects sufficient, we will describe three models, which can explain main properties. If we don't quote different, the formulas used in this chapter are from [1].

#### 2.1.1. Drop model

The main adoption of the drop model is, that a core has properties, that are similar to those of a drop of water. The water molecules can be associated to the nucleons. This model is especially useful to calculate the binding energy. This can get calculated with the help of the following formula, where  $A$  is the number of nucleons and  $Z$  is the number of protons.  $N$  is the number of neutrons and  $a_j$  are constants.

$$E_B = \underbrace{a_V \cdot A}_{1)} - \underbrace{a_O \cdot A^{2/3}}_{2)} - \underbrace{a_C \cdot Z^2/A^{1/3}}_{3)} - \underbrace{a_A \cdot (N - Z)^2/A}_{4)} \pm \underbrace{a_P \cdot A^{-3/4}}_{5)}, \quad (2.1)$$

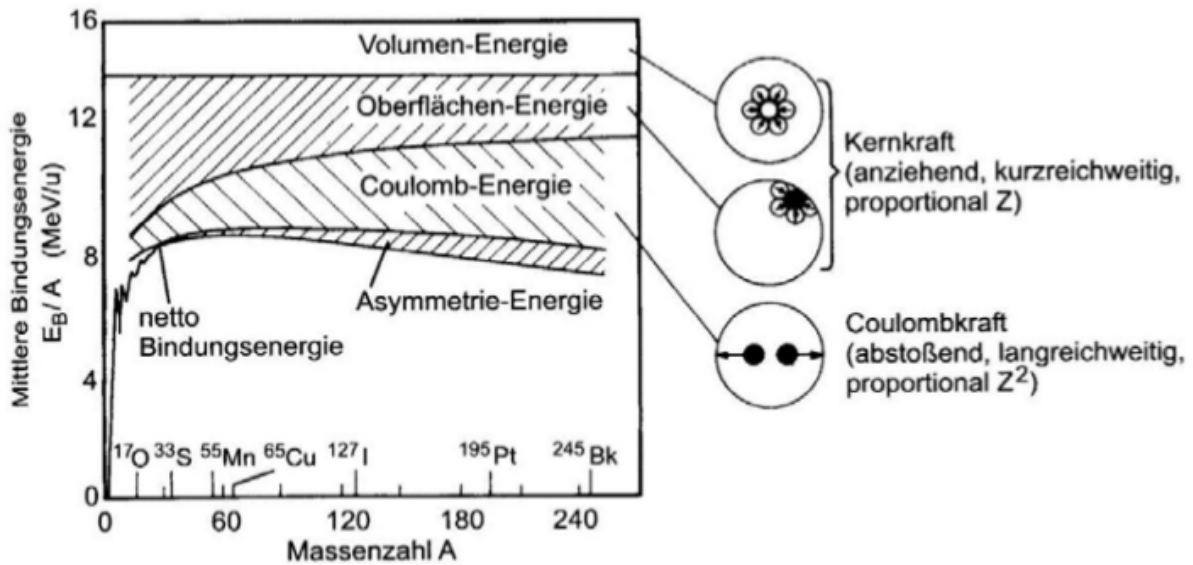


Figure 1: Terms of the binding energy as function of the mass number  $A$ .  
[1, S.8]

with a term 1), which takes the volume into account. 2) is the surface term, which describes, that the binding energy is weaker at the surface. 3) is called the coulomb-term. It describes, that positive charged nucleons push each other apart. The asymmetry term 4) says, that light cores with the same number of protons and neutrons are very stable and heavy cores with  $A \geq 40$  and  $Z = N$  get unstable. 5) is the so called pair term. It describes, what happens if cores are gg-, ug- or uu-cores. g means an even number of nucleons of one type, u an odd one (see [3]). The single components of the energy and the resulting total energy are plotted in Figure 1. From this energy the Weizsäcker-mass-formula can be derived, which gives the the mass of an atom

$$M(A, Z) = (A - Z) \cdot m(n) + Z \cdot m(p) + E_B/c^2 + Z \cdot m_e. \quad (2.2)$$

$m(p)$  is the mass of a proton,  $m(n)$  that of a neutron and  $m_e$  that of an electron.  $c$  is the speed of light.

### 2.1.2. Fermi-gas-model

The difference to the drop model, which is a classical model, is that now quantum mechanical effects are taken into account. It is assumed, that the core is a gas made up of free neutrons and protons. Both of them are fermions, which means, that they have a spin of  $1/2$ . Because of this they have to obey the Pauli-principle, which allows for each energy level in a potential to host only two nucleons of one type (see Figure 2). The highest level with nucleons is called Fermi-level  $E_F$ .

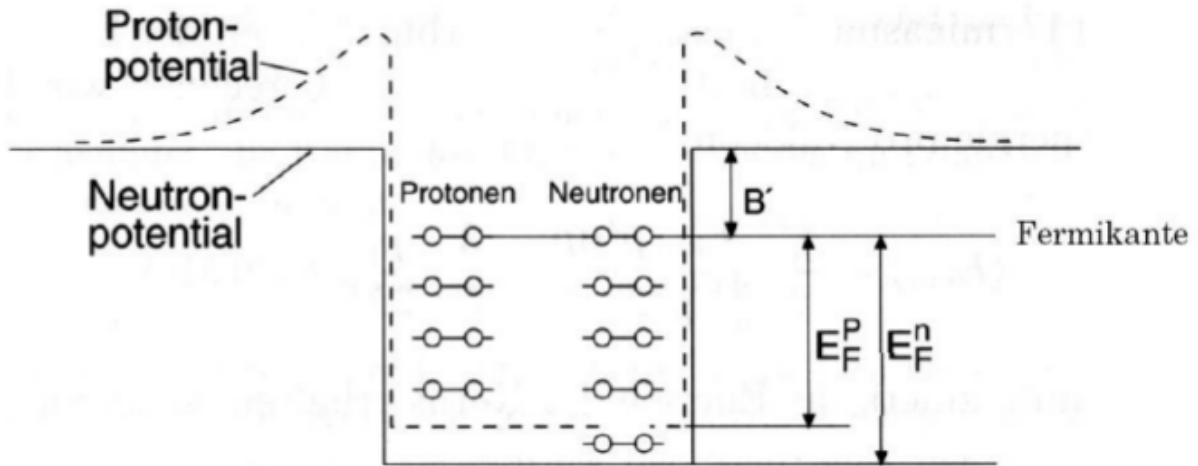


Figure 2: Proton and neutron core potential.

[1, S.9]

It can be seen, that the potentials for neutrons and protons are different. The reason for this is the Coulomb force, which only affects the protons.

### 2.2. Shell model

This model is analogue to the electron shell model. Here the nucleons are on discrete shells in the core. On each of those shells a special number of nucleons finds space. This model allows to describe the fine structure, the magnetic moment and the excitation energy. Furthermore this model can explain the irregularities which can be seen for small mass numbers in Figure 1. They are described by the Magic Numbers.

### 2.3. Radioactive decay

A radioactive decay is a statistical process. The decrease is proportional to the number of existing cores  $N$

$$\frac{dN}{dt} = -\lambda N. \quad (2.3)$$

This is a differential equation with the solution

$$N(t) = N_0 e^{-\lambda t} \quad (2.4)$$

(see [4]).  $\lambda$  is called decay constant. It gives, which fraction of the original material decays per time interval. If there are more than one decay channels possible, the decay constants get added.

The time, after which half of all cores of a sample are decayed, is called half-life period. It can be calculated with

$$T_{1/2} = \frac{\ln 2}{\lambda}. \quad (2.5)$$

The average life time, which can be derived from the timely expected value, is given as

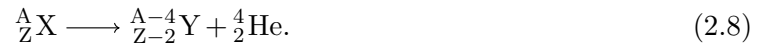
$$\tau = \frac{1}{\lambda} = \frac{T_{1/2}}{\ln 2}. \quad (2.6)$$

The activity is defined with the number of decays per time interval

$$A = \lambda N = \frac{N}{\tau}. \quad (2.7)$$

#### 2.4. $\alpha$ -decay

At the  $\alpha$ -decay the core splits in a lighter core and a helium atom



Classically such a transition isn't possible, since a  $\alpha$ -particle doesn't have enough energy in order to leave the core. This only can be explained with quantum mechanic. The nucleons of the  $\alpha$ -particle are tunnelling through the potential of the protons out of the core (see Figure 2).

#### 2.5. $\beta$ -decay

There are tree types of  $\beta$ -decays. All of them have in common, that the mass number  $A$  stays constant, but the atomic number  $Z$  changes around one. Electric charge, Baryon- and Lepton-number must be conserved.

##### $\beta^-$ -decay

At the  $\beta^-$ -decay a neutron becomes a proton, a electron and an anti-electron-neutrino

$$n \rightarrow p + e^- + \bar{\nu}_e, \quad (2.9)$$

where it is very difficult to detect the anti-neutrino, like the neutrinos. The interaction particle in this process is a  $W^-$ -particle.

##### $\beta^+$ -decay

Another possible decay process is the  $\beta^+$ -decay. This happens not as often as the  $\beta^-$ -decay. Here a proton gets transformed into a neutron, a positron and an electron-neutrino, while exchanging a  $W^+$ -particle

$$p \rightarrow n + e^+ + \nu_e. \quad (2.10)$$

The positron can't exist free if there is mater around. It combines with an electron to a positronium. This has a half-life time of  $10^{-7}$  bis  $10^{-9}$  s. In this decay two, sometimes three, photons get freed. In a decay where two  $\gamma$ -quanta get free, both of them have an energy of 0.511 MeV. Because of the conservation of momentum, the angle between their trajectories is  $180^\circ$ .

### Electron capture

This effect is especially relevant for heavy atoms. Here an electron from the lowest shell, the K-shell, gets caught by the core

$$p + e^- \rightarrow n + \nu_e. \quad (2.11)$$

In its place comes a photon of one of the higher shells. The energy, that gets free, can be emitted as X-ray or with the Auger-effect.

### 2.6. $\gamma$ -decay

The  $\gamma$ -decay happens at atoms, which fall back to the ground state, if they haven't enough energy to be able to emit particles. The energy gets emitted in form of electro-magnetic rays. The photons of these rays have an energy of  $E = h\nu$ . This decay process takes place in a range of nano- and femto-seconds. The energy of the  $\gamma$ -quanta is at keV to MeV.

### 2.7. Inner conversion

Instead of  $\gamma$ -radiation the excitation energy  $E_\gamma$  can be given directly to an electron in the shells. This gets pushed with the energy difference of excitation energy and binding energy away from the core

$$E_e = E_\gamma - E_B. \quad (2.12)$$

The gap, that exists then gets closed by an electron from a higher shell. By this process X-rays get sent out.

### 2.8. Interaction of electromagnetic radiation with matter

There are three important processes, which are responsible for the interaction between electromagnetic radiation and matter: the photo effect, the Compton effect and the pair coupling. The intensity of a photon beam decreases exponentially, depending on the absorption coefficient, in matter. Which process is favoured by which energy can be seen in Figure 3.

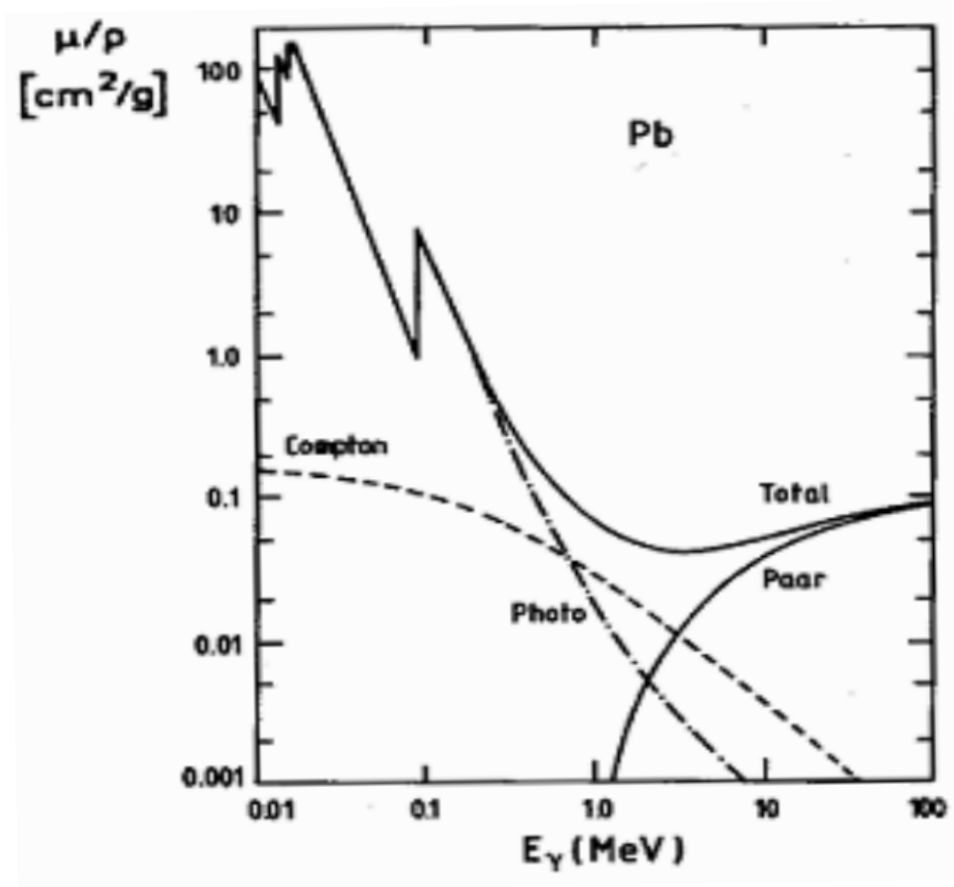


Figure 3: Mass absorption coefficient for photons in lead.  
[1, S.28]

### 2.8.1. Photo effect

Photons can kick electrons out of the shell of the atom. If the Photon has an energy of  $E = h\nu$ , then is the energy of the now free electron

$$E = h\nu - E_B, \quad (2.13)$$

with the binding energy  $E_B$ . In Figure 3 can be seen, that the curve of the photo effect has some peaks. The reason for this is, that the photo effect is most probable for photons which have the same energy as the binding energy in the shell, from which the electron came.

### 2.8.2. Compton effect

The Compton effect describes the dispersion of a photon on an electron. The electron is free or only weak bound. The photon transfers a part of its energy on the electron. The energy, which the photon has after the dispersion, depends on the rest mass of the electron, the speed of light and the scattering angle.

### 2.8.3. Pair coupling

If a photon has at least the double of the resting energy of an electron, then pair coupling is possible in the field of an atomic core. In this process an electron-positron-pair is produced out of the photon. The core takes the recoil energy. Since a positron can't exist freely, it has to annihilate again with an electron. By doing this  $\gamma$ -quanta get free.



## 2.9. Used radioactive samples

### 2.9.1. $^{22}\text{Na}$

The half life time of  $^{22}\text{Na}$  is  $T_{1/2}(^{22}\text{Na}) = 2.6088\text{a}$ . It decays nearly with 100% over  $\beta$ -decay in the excited state  $2^+$  of  $^{22}\text{Ne}$ .  $\beta^+$  happens with a probability of 89.9% and electron capture with 10.1%.



There are two intensive lines in this spectrum: one at 511 keV and one at 1274.6 keV. The first is an annihilation peak, in the second the excited state goes to the ground state while sending out a  $\gamma$ -quantum.

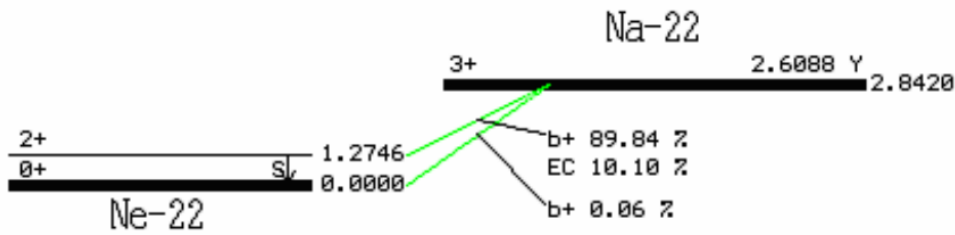


Figure 4: Decay scheme of  $^{22}\text{Na}$ . Energies are in keV [1].

### 2.9.2. $^{60}\text{Co}$

Nearly all  $^{60}\text{Co}$  decays with a half life time of  $T_{1/2}(^{60}\text{Co}) = 5.2714\text{a}$  in the third excited state  $4^+$  of  $^{60}\text{Ni}$



There are two very intensive lines. The most probable transition is that from the excited state  $4^+$  to  $2^+$ . The energy difference is 1173.2 keV. 0.7 ps after that transition another  $\gamma$ -quantum gets free. It has an energy of 1332.5 keV and brings the electron to the ground state.

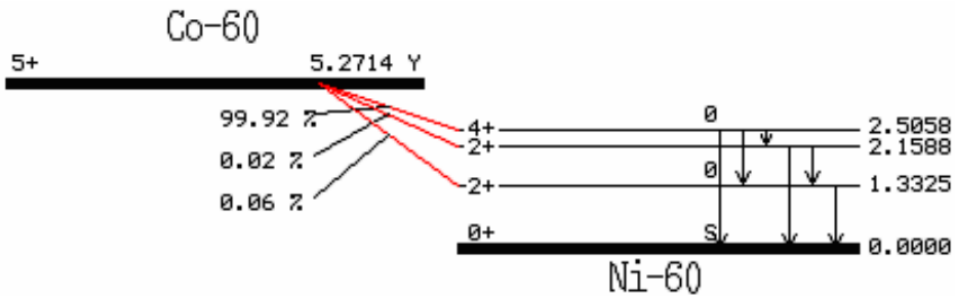


Figure 5: Decay scheme of  $^{60}\text{Co}$ . Energies are in keV [1].

### 2.9.3. $^{152}\text{Eu}$

The half life time of  $^{152}\text{Eu}$  is  $T_{1/2}(^{152}\text{Eu}) = 12\text{a}$ . All three types of decay are possible:





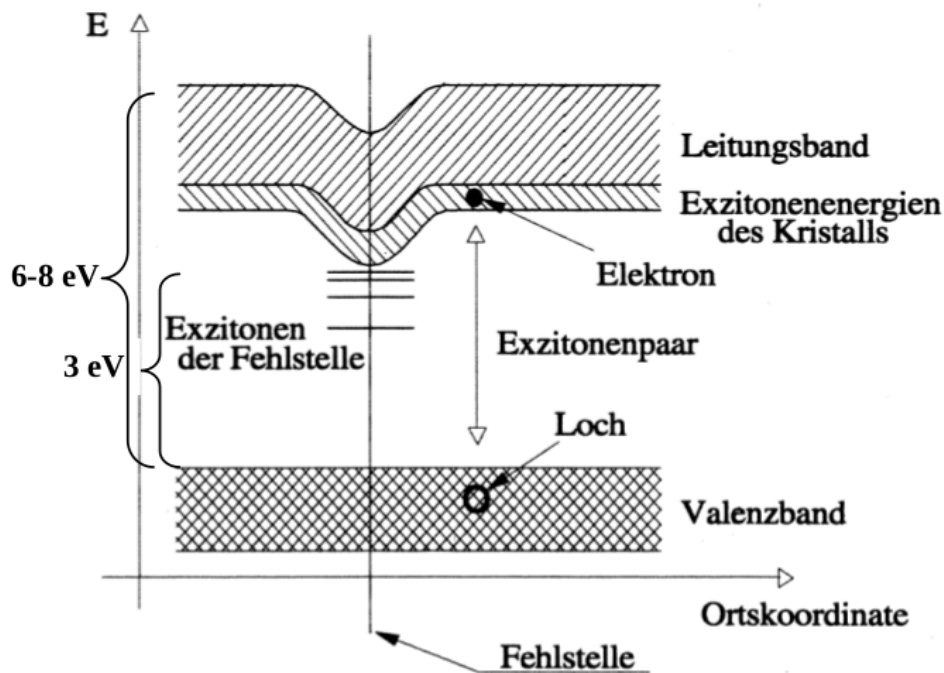


Figure 8: Band structure in an inorganic scintillator [1].

Because of the doping of the material, in our case with Thallium, the electron falls back to the valence band over different energy levels. If the material wouldn't be doped, the photons that get emitted by the decay would excite another electron and they wouldn't leave the scintillator so easily. The detection of the photons is done with a photo multiplier. They are mostly used if a high energy resolution is needed.

### 2.10.2. Organic scintillators

Organic scintillators can be made of organic liquids, compounds or plastic. We use the last type. They work by energy transitions between molecular orbitals. They are often used for time measurements. Furthermore it is possible to detect neutrons with them and they are quite resistant against damage by radiation.

### 2.10.3. Photo multiplier

Photo multipliers are used to transform incoming photons in a voltage signal, which we can measure. The setup can be seen in Figure 9.

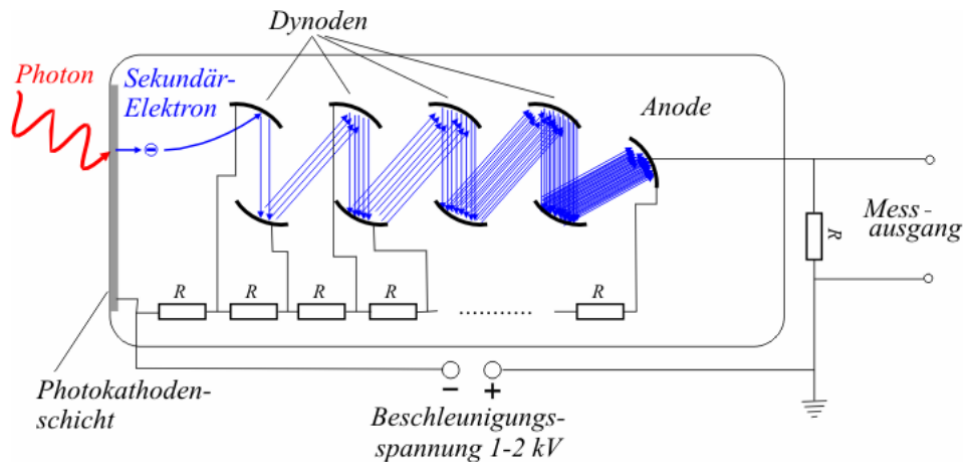


Figure 9: Scheme of a photo multiplier [1].

A photon hits an electron out of the photo cathode because of the photo effect. This electron gets accelerated to a dynode, where it knocks out further electrons, which again accelerate against a dynode, and so forth until the electrons reach the anode, where a voltage is measurable.

#### 2.10.4. Pre- and main-amplifier (PA/MA)

The reason why PAs are used is, to increase the signal of the detector. Since the signals of the detector is very weak, the PA has to be set near the detector in order to minimise the length of the wire. With this setup the influence of scattering field or wire capacities are minimised and the property between the signal and noise get enhanced. The signal after the PA is an exponential signal with a long sloping end.

In a MA the signal of the PA gets further enlarged and the form of the signal gets changed (pulse shaping). If the interesting information is the time, the MA has to answer quickly. If the experimenter is interested in the height of the peak, a linear dependence between the incoming and the outgoing signal is needed.

#### 2.10.5. Single and multi channel analyzer (SCA/MCA)

The SCA can give an output for a signal, that lies in a range of energy, that can be adjusted. In the MCA the pluses get sorted into channels. In which channel they come, depends on their amplitude. The determination, which channel is associated to which energy, can be done by comparing known energies to measured peaks.

### 3. Setup and procedure

#### Setup

Since this experiment consists of two parts, there are two setups. The instruments used in them can be seen in Figure 10. In the first part only a NaI-scintillator is used to measure the spectrum of  $^{228}\text{Th}$ . In the second part a plastic scintillator is used additional, in order to measure the angle distribution of annihilation photons.

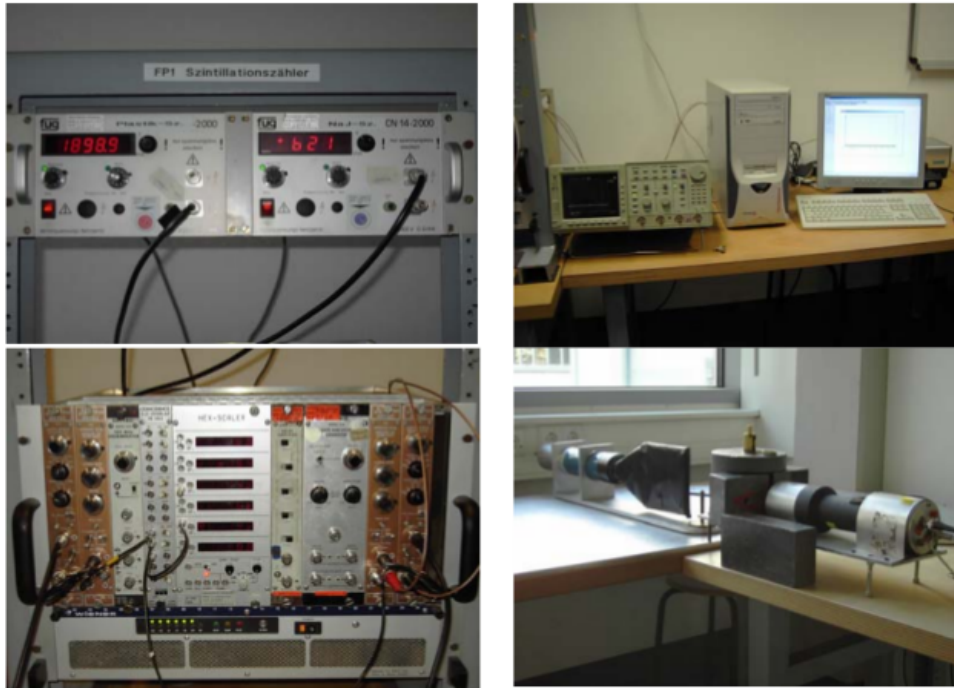


Figure 10: Setup of the experiment [1].

#### Measurement of the $^{228}\text{Th}$ -spectrum

The setup for the calibration of the energy and the measurement of the  $^{228}\text{Th}$ -spectrum can be seen in Figure 11.

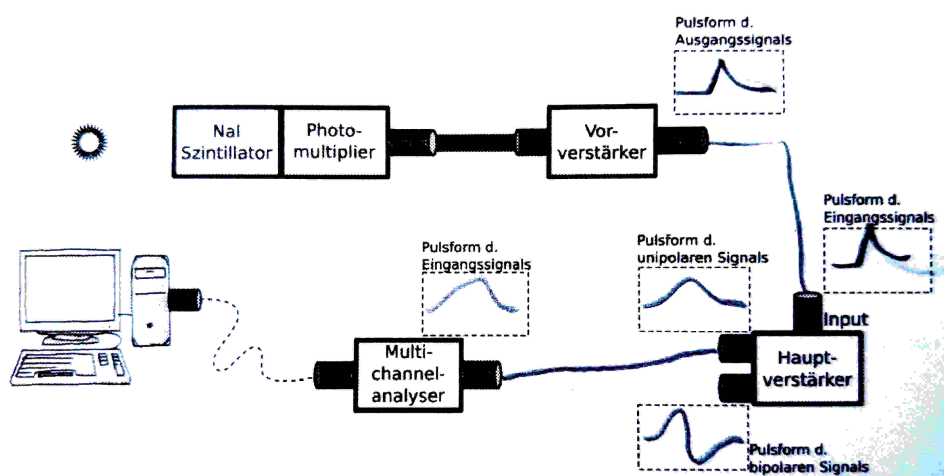


Figure 11: Block diagram for the measurement of the first part of the experiment [2].

A photo multiplier transforms the signal, which comes from the scintillator in an electric signal.

This signal gets amplified by a preamplifier and the main amplifier, which also shapes the signal from a slow decaying signal to a signal with one peak. The multi channel analyser analyses the spectrum and sorts it into channels which can be measured. The isotopes, that are used for the calibration are  $^{22}\text{Na}$ ,  $^{60}\text{Co}$  and  $^{152}\text{Eu}$ .

### Coincidence Measurement

In the second measurement a sample of  $^{22}\text{Na}$  is brought between the organic and the inorganic one. The block diagram for this is shown in Figure 12. A picture of our real setup can be found in the appendix in Figure 37.

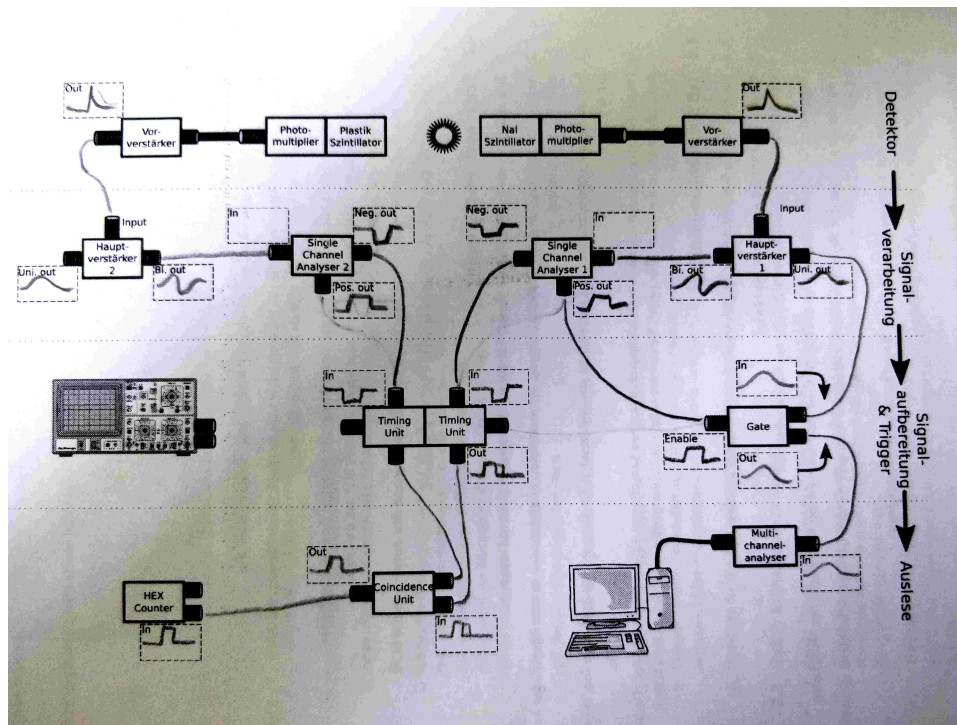


Figure 12: Block diagram for the measurement of the second part of the experiment [2].

The plastic scintillator is movable in a section of a circle around the sample. For setting the angle there are carvings each  $5^\circ$ . Close to  $0^\circ$  there are pencil markings at each degree. The signals get transformed into rectangular signals with the single channel analyser. In the coincidence unit it is measured, how often the signals from both scintillators overlap. Previous to this the energy window has to be set, so that only the annihilation photons with an energy of 511 keV of the  $^{22}\text{Na}$  decay get measured.

### Procedure

We started our measurement with taking the signal sequences of the used tools. For this the  $^{22}\text{Na}$  sample was used. The sequences were looked at with an oscilloscope. This was done in order to find the optimal settings for the following measurements. Then we measured the spectra of the europium, the cobalt and the sodium sample. The first one was measured approximately 40 min, the others 30 min. We then did the coincidence measurement in a range from  $-90^\circ$  to  $90^\circ$ . We also measured the background for the coincidence. This was done 100 s. After that we measured the spectrum of thorium over night for about 15 h. Finally the background was measured with the inorganic scintillator. This was done for about 3 h.

## 4. Data analysis

The analysis of the data was done using Python. For fit functions we used the least-square-fit function `curve_fit` from the `scipy.optimize` package. Some plots won't have errorbars in them. That's due to the fact, that they are either too small to be visible or we omitted them on purpose for the sake of clarity.

### 4.1. Preparation

For the experiments we first needed to set everything properly. To do so, we looked at the signals after each module on the oscilloscope.

First we looked at the signal from the preamplifier (see Figure 13). From this we can read off the time constant we need to set in the main amp. It is the duration of the signal to drop down. We measured about  $3\ \mu\text{s}$ .

In Figure 14 to 19 we looked at the effect of the shaping time on the unipolar signal after the main amplifier. We can see, that with a higher shaping time the signals tend to become more of a bipolar signal shape. At  $3\ \mu\text{s}$  we have the sweet spot between having a thin signal and an unipolar looking one. In Figure 20 we looked at the bipolar output from our main amplifier.

In Figure 21 we looked at the signal from the organic scintillator from after the preamplifier and proceeded with the same setup method as with the inorganic detector.

In Figure 23 and 24 we looked at the single channel analyser positive and negative signal outputs. We looked at the negative signals from the organic and inorganic detectors on the oscilloscope, to set the delay for the signals. Sadly we forgot to take pictures of this step.

We also looked at the signal from after the gate, and got the same signal from before the gate. We also forgot to take pictures there.

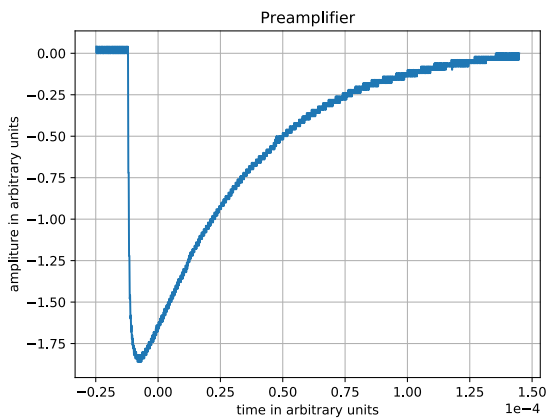


Figure 13: Negative signal from the preamplifier of the NaI detector.

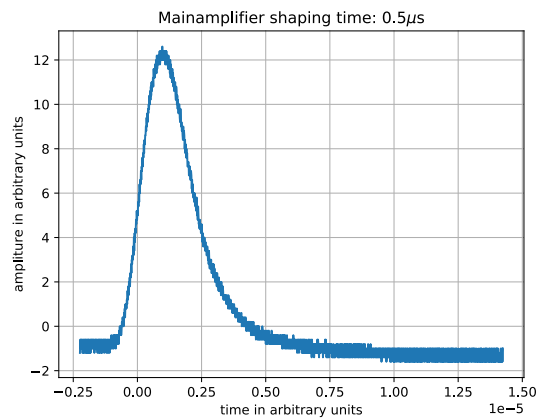


Figure 14: Signal from after the mainamplifier with  $\tau = 0.5\ \mu\text{s}$ .

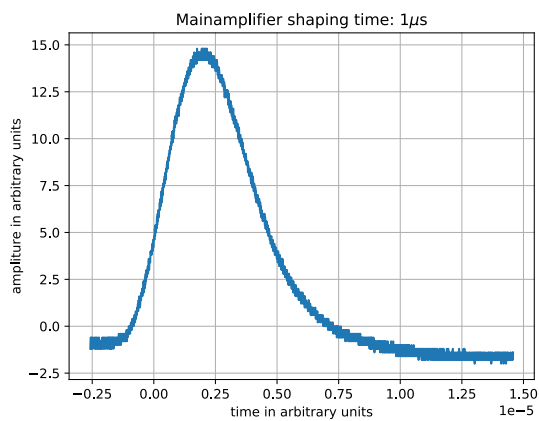


Figure 15: Signal from after the mainamplifier with  $\tau = 1 \mu\text{s}$ .

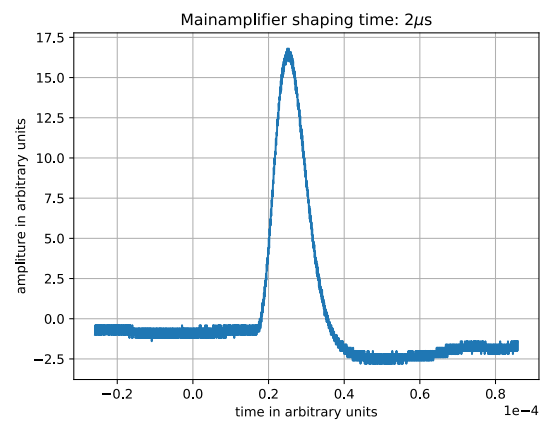


Figure 16: Signal from after the mainamplifier with  $\tau = 2 \mu\text{s}$ .

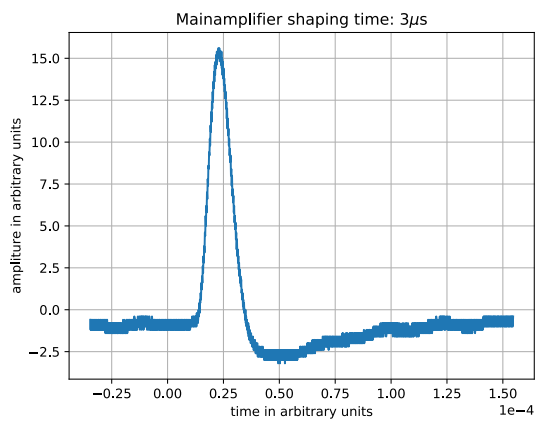


Figure 17: Signal from after the mainamplifier with  $\tau = 3 \mu\text{s}$ .

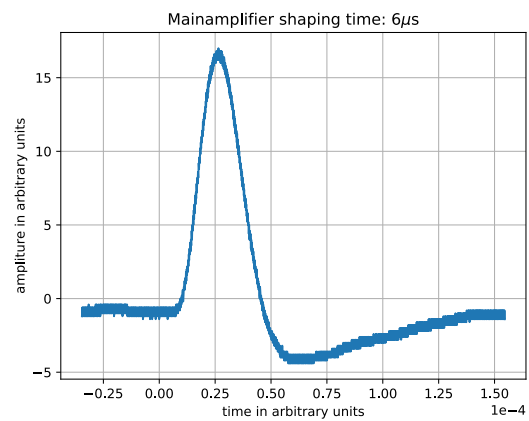


Figure 18: Signal from after the mainamplifier with  $\tau = 6 \mu\text{s}$ .

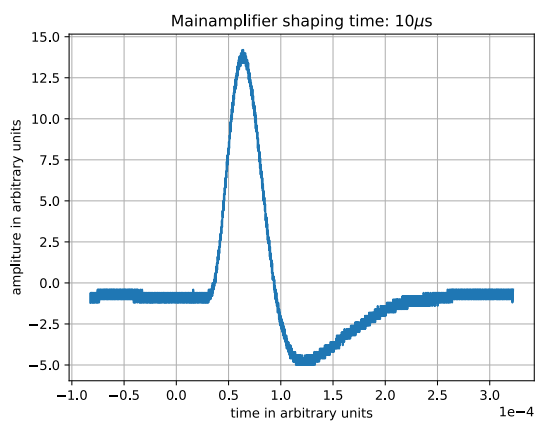


Figure 19: Signal from after the mainamplifier with  $\tau = 10 \mu\text{s}$ .

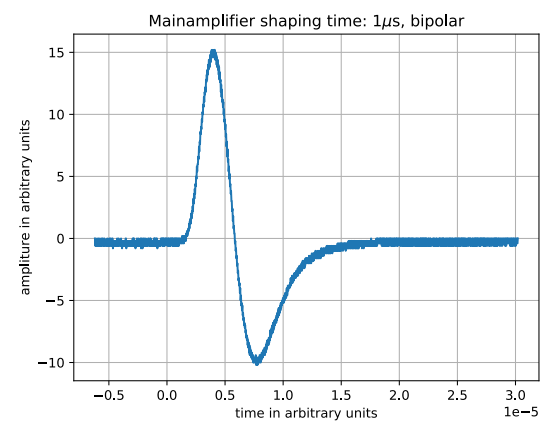


Figure 20: Bipolar signal from after the mainamplifier with  $\tau = 1 \mu\text{s}$ .



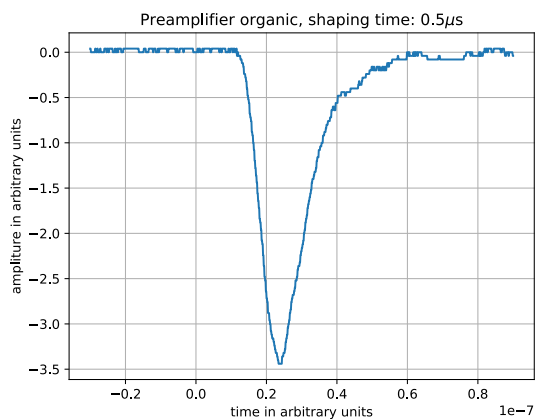


Figure 21: Negative signal from the preamplifier of the organic detector.

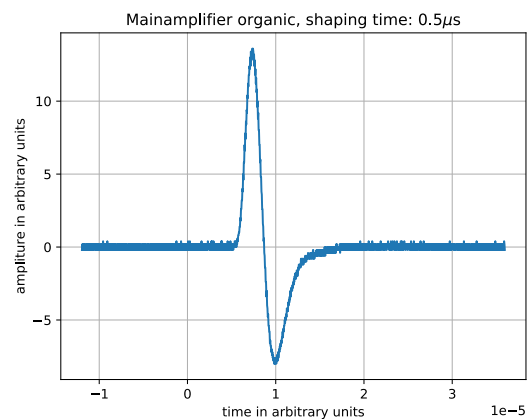


Figure 22: Bipolar signal from after the mainamplifier with  $\tau = 0.5\mu\text{s}$ .

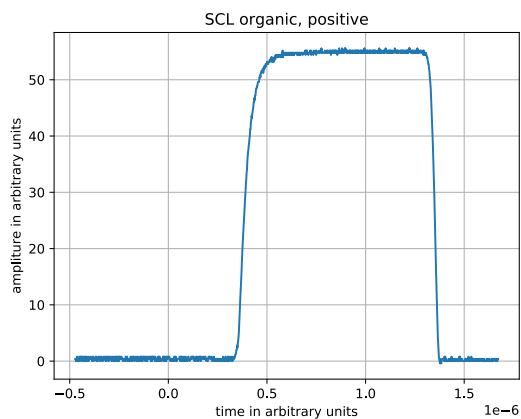


Figure 23: Positive signal output from after the SCL.

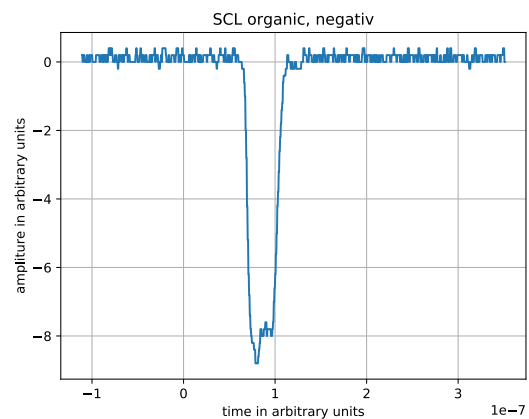


Figure 24: Negative signal output from after the SCL.

## 4.2. Background measurement

The background we measured is plotted in Figure 25. The error on the number of counts  $N$ , can be calculated as  $s_N = \sqrt{N}$ . This is due to the fact, that we assume a Poisson distribution. When we did this, it could be seen, that they are too small to be seen in the plot.

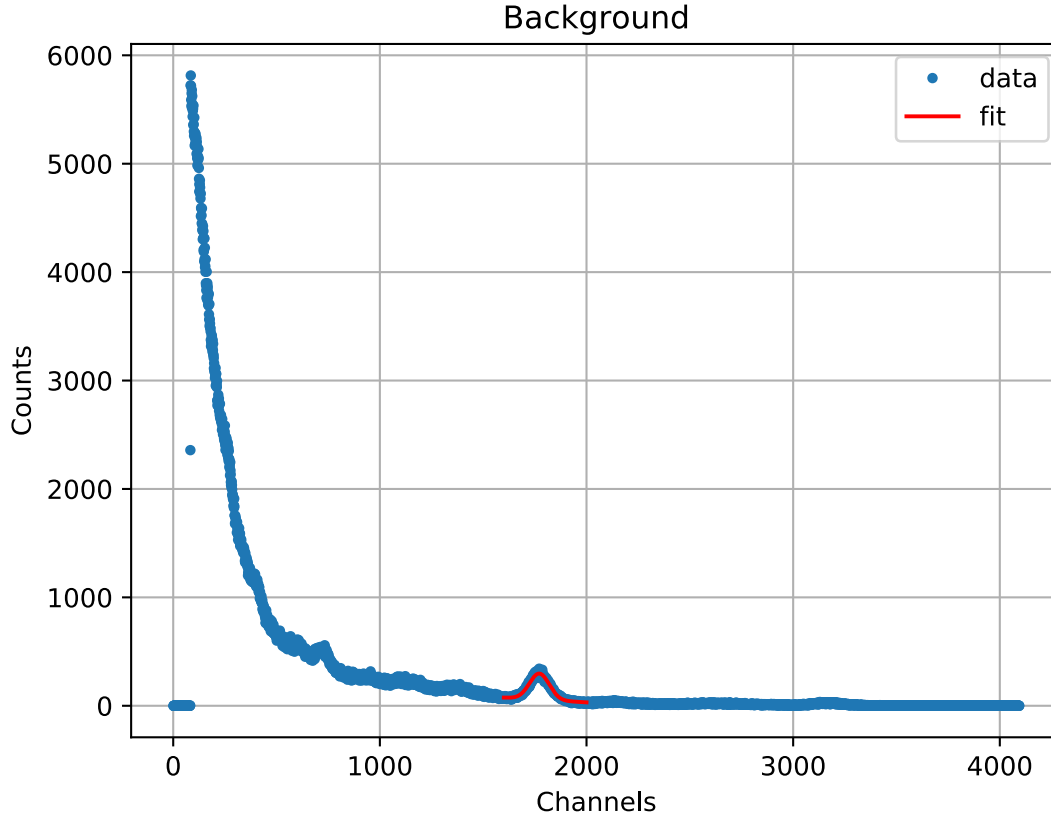


Figure 25: Background data with fitted peak.

There is a peak a bit underneath the 2000<sup>th</sup> channel. We fit a Gaussian function of the form

$$f(x) = a \cdot e^{-\frac{(x - \mu)^2}{2\sigma^2}} + bx + c \quad (4.1)$$

to this peak. This formula will be used for all the following fits to peaks. We get, that the peak is in channel  $1771.6 \pm 0.4$ . With the energy-channel relation, which we will derive later, we get, that this is an energy of  $E = (1465 \pm 5)$  keV. With these data we were able to subtract the background from the spectra. Because the background was measured for  $t_{\text{back}} = 3.56$  h, and the spectra only for between 30 min and 40 min, the background had to be normalised. This was done by calculating

$$N_U = \frac{N_{U, \text{alt}} \cdot t_{\text{spect}}}{t_{\text{back}}} \quad (4.2)$$

Because of this the error on the number of counts must get propagated

$$s_N = \sqrt{s_{NU} + s_N}. \quad (4.3)$$

### 4.3. Characterisation of the MCA

We measured the spectra of sodium, europium and cobalt. The reason for this is, that for each of these spectra two characteristic energy peaks are known from [1]. This allows to compare a channel number with an energy. Figure 26 shows our measured spectrum of sodium. In all these graphs the background is subtracted.

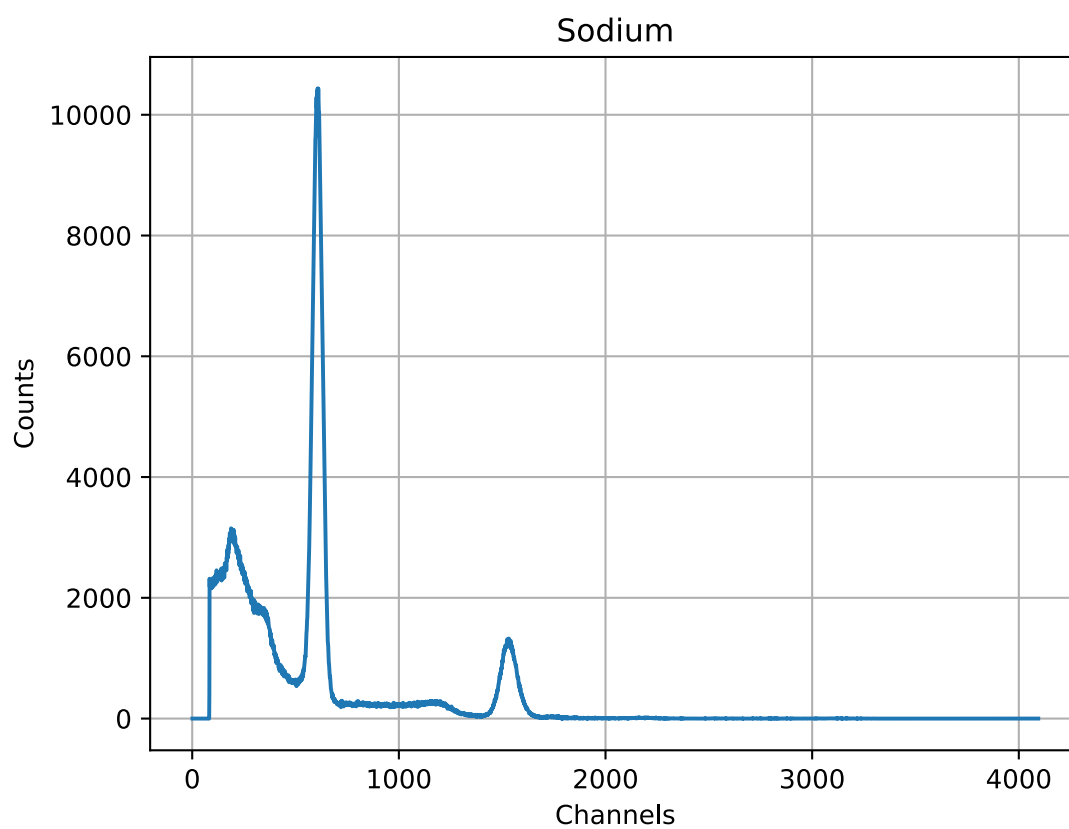


Figure 26: Total sodium spectrum without background.

In Figure 27 The two peaks, that we associate with the energies from literature are enlarged and fitted with Equation 4.1.

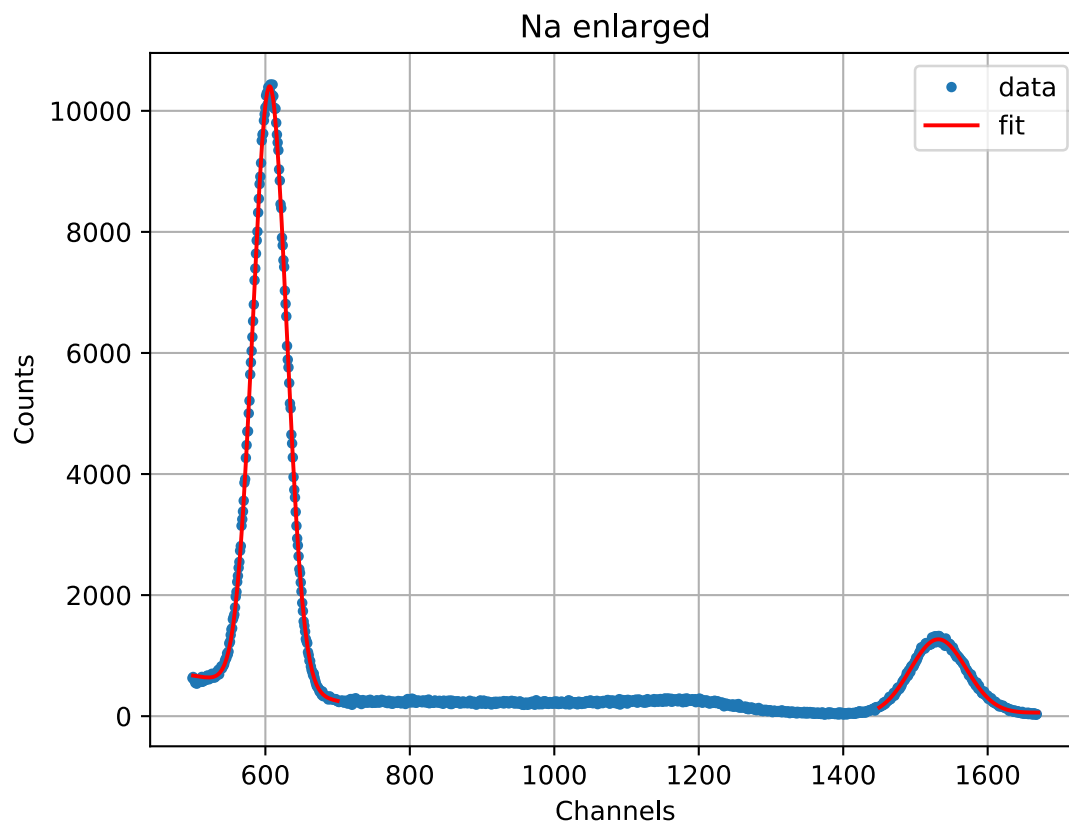


Figure 27: Characteristic peaks in the sodium spectrum without background.

The result can be seen in Table 1.

Channel	Energy [keV]
$606.00 \pm 0.04$	511
$1531.5 \pm 0.2$	1274.6

Table 1: Peaks in the spectrum of sodium without background.

The total measured data of the spectra of europium and cobalt can be found in the appendix in Figure 38 and Figure 39. Here we just show their characteristic peaks. They can be seen in Figure 28 and Figure 29. The corresponding energies are listed in Table 2 and Table 3.

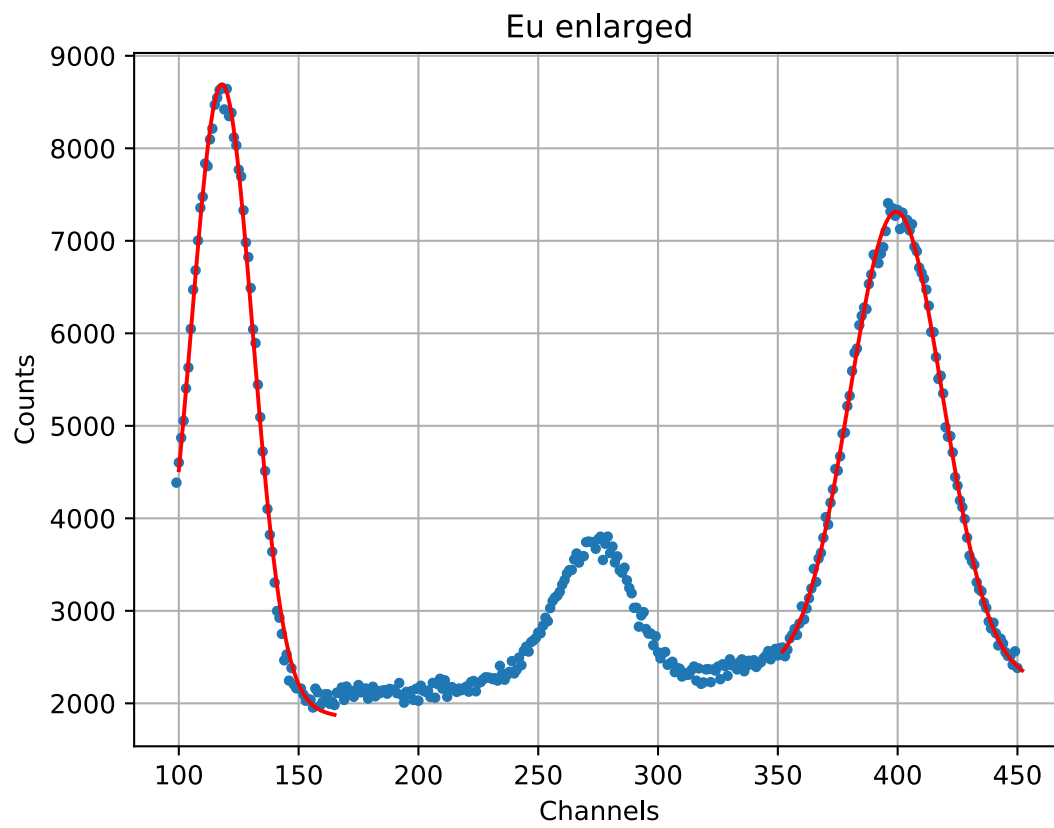


Figure 28: Characteristic peaks in the europium spectrum without background.

Channel	Energy [keV]
$118.1 \pm 0.2$	122
$399.44 \pm 0.11$	344

Table 2: Peaks in the spectrum of europium without background.

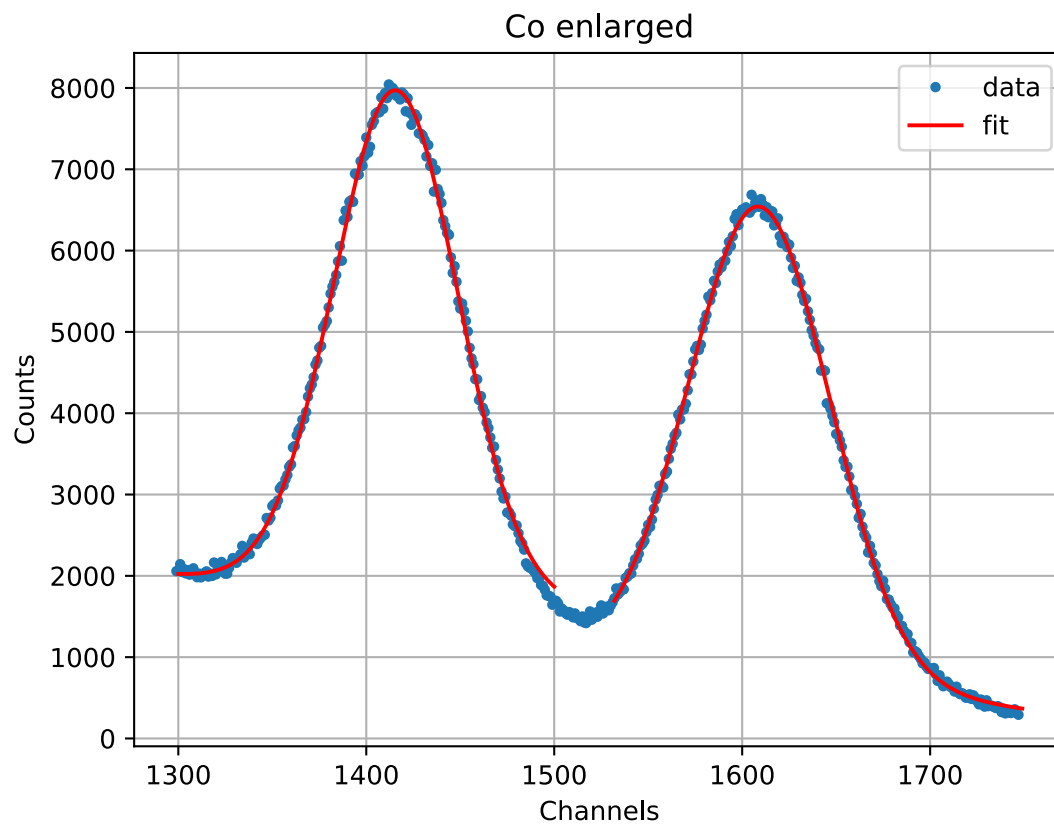


Figure 29: Characteristic peaks in the cobalt spectrum without background.

Channel	Energy [keV]
$1415.7 \pm 0.2$	1173.2
$1609.12 \pm 0.11$	1332.5

Table 3: Peaks in the spectrum of cobalt.

These channels get plotted against the energies. This is shown in Figure 30.

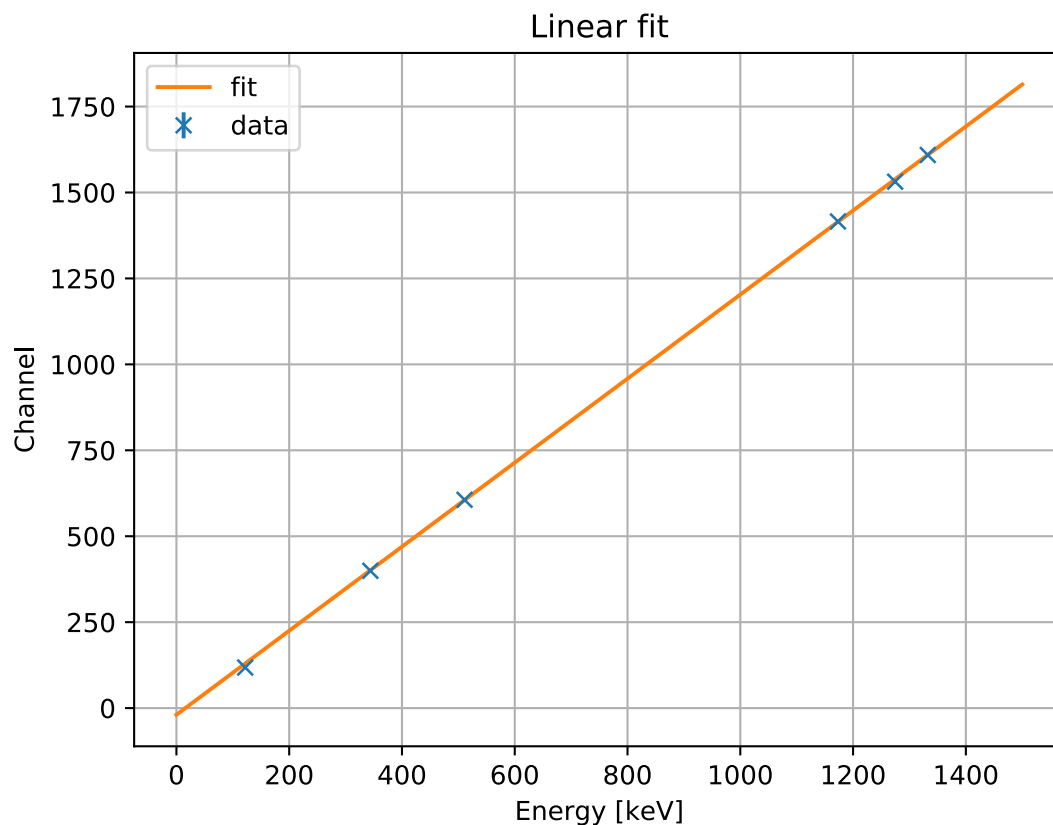


Figure 30: Linear calibration of the MCA.

The fit through the data is a linear function

$$C(E) = a \cdot E + b. \quad (4.4)$$

With our data we got as fit factors

$$a = (1.222 \pm 0.004) \text{ counts/keV} \quad (4.5)$$

$$b = -(19 \pm 2) \text{ counts} \quad (4.6)$$

with  $\chi^2 = 1.095$ . This allows to calculate energies out of channels.

#### 4.4. Energy spectrum of the $^{228}\text{Th}$ decay

The things we did in the previous chapter were mainly done, so that we are now able to analyse the spectrum of thorium. In Figure 31 the total spectrum, our measured data minus the background, can be seen. The data of the channels 0 to 83 isn't plotted, because there the number of counts had been unchanged at zero. Here we have, using Equation 4.4, changed the x-axis from channels to energy. This allows to see at which energies there are peaks.

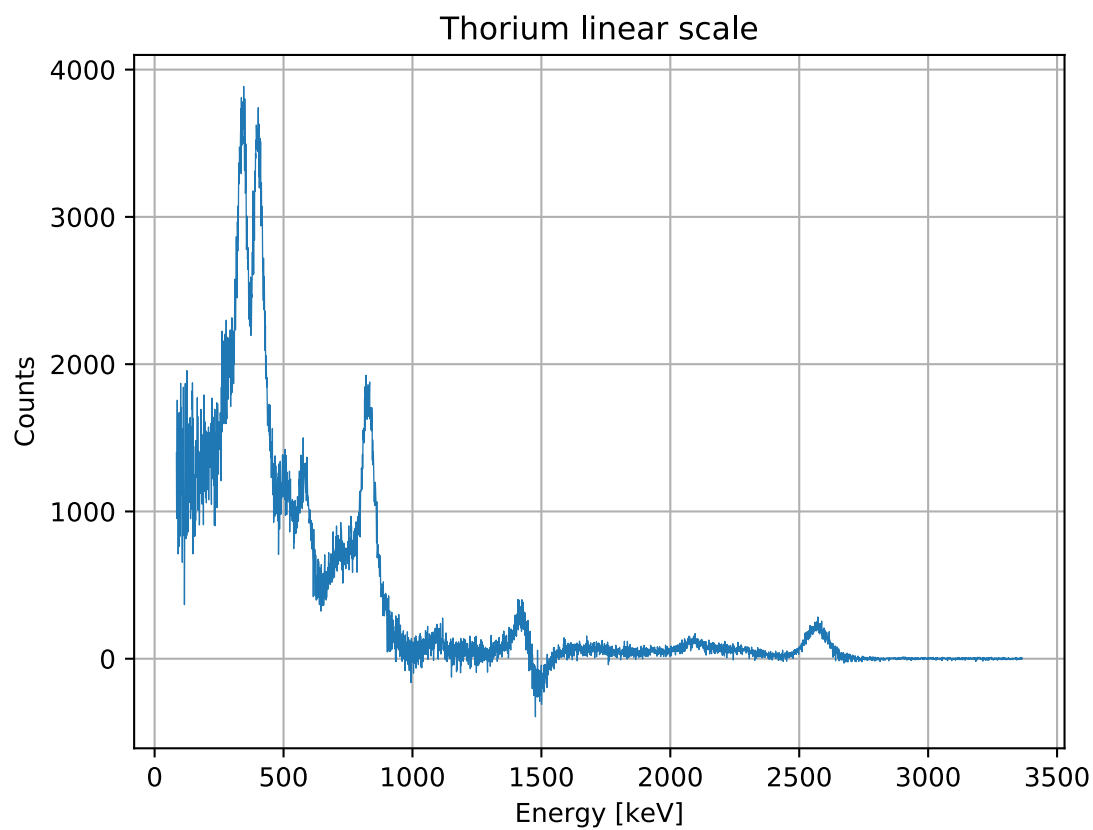


Figure 31: Total thorium spectrum without background.

In the appendix a picture of the same data can be found (Figure 40), where we used a logarithmic scale in y-direction. Some peaks are more clear there. In order to find the energies of the peaks, we plot again Gaussian functions to them. This is shown in Figure 32 to Figure 35.



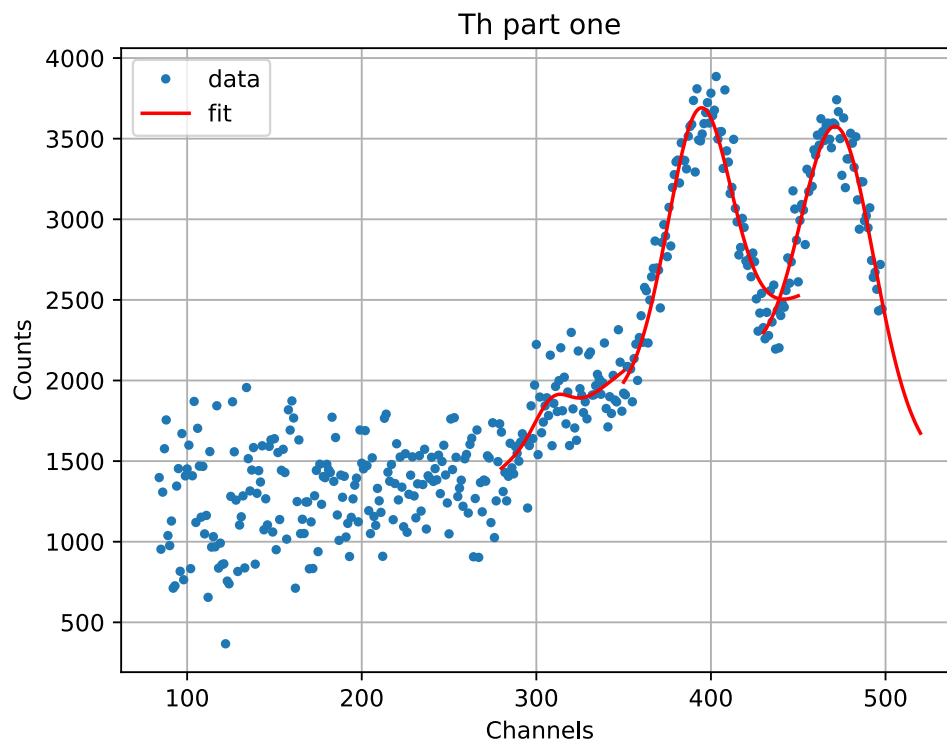


Figure 32: Part one of the spectrum of Thorium without background.

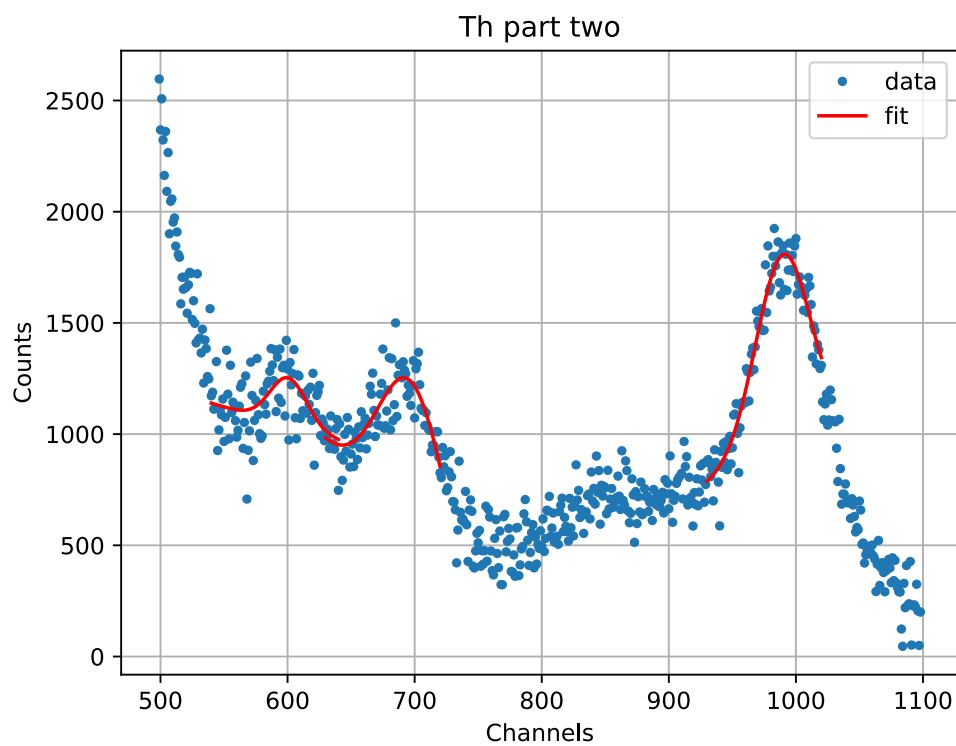


Figure 33: Part two of the spectrum of Thorium without background.

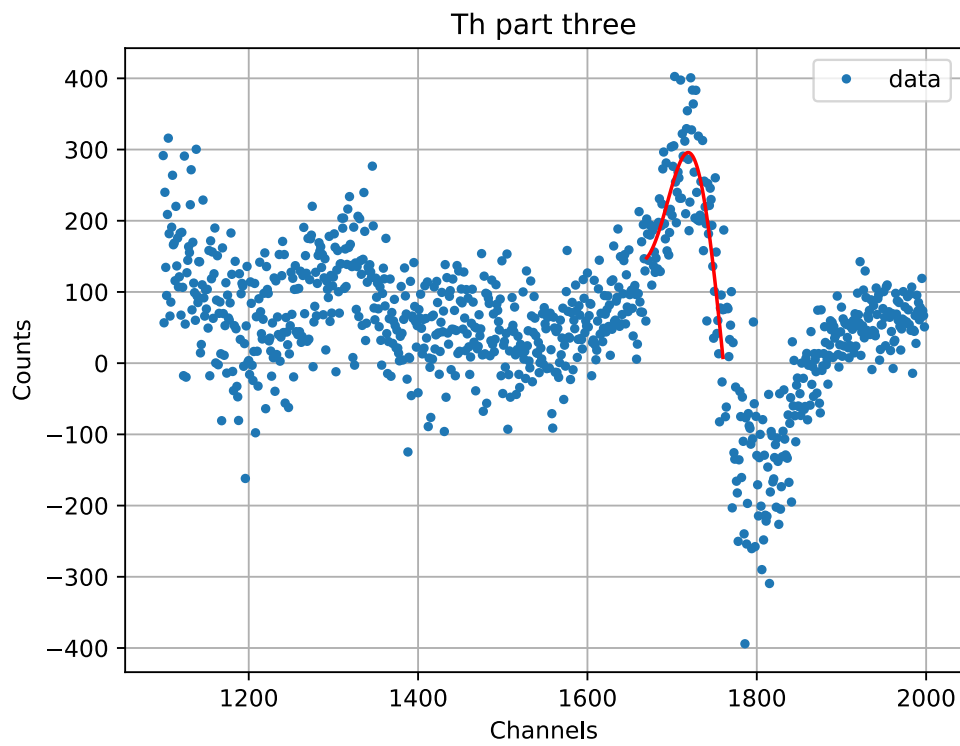


Figure 34: Part three of the spectrum of Thorium without background.

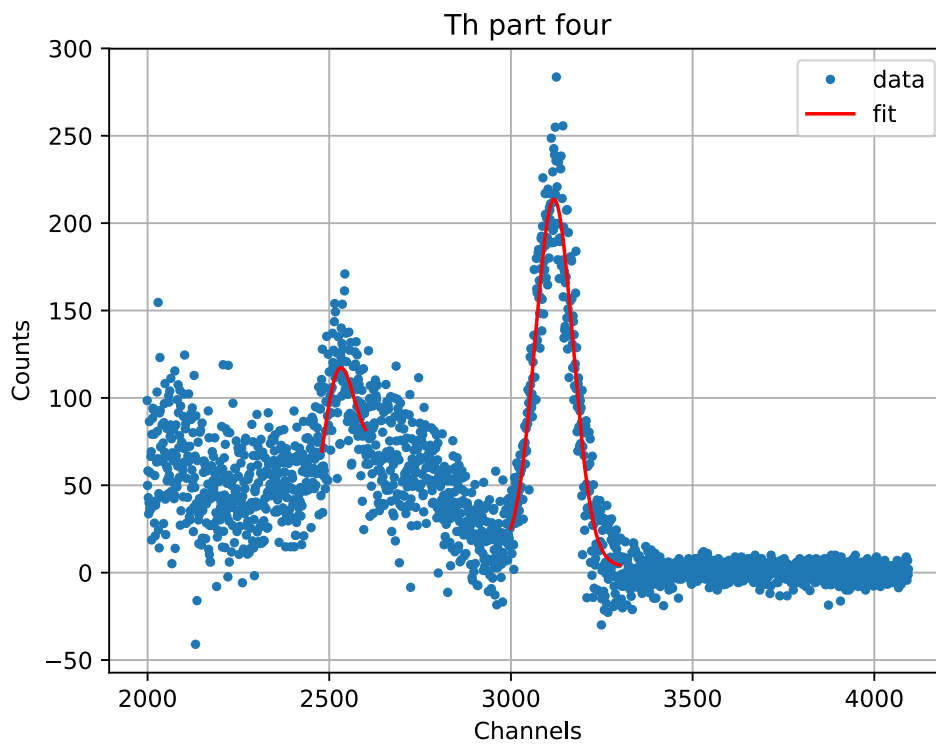


Figure 35: Part four of the spectrum of Thorium without background.

Thanks to Equation 4.4, we are able to calculate energies out of these channels. The results are listed in Table 4.

Channel	Energy keV	Theoretical transition	Deviation
$309 \pm 4$	$269 \pm 4$	$^{228}\text{Tl}(277.36 \text{ keV})$	$3\sigma$
$393.4 \pm 0.8$	$338 \pm 2$	$^{212}\text{Pb}(300.09 \text{ keV})$ , it has systematically a higher energy because of the Compton effect of the following peak	$19\sigma$
$472.5 \pm 0.7$	$402 \pm 2$	$^{212}\text{Bi}(452.98 \text{ keV})$ , it has systematically a lower energy because of the uncertainty resulting from the asymmetry of the fit, that is induced by the following peak	$26\sigma$
$601 \pm 3$	$507 \pm 4$	$^{208}\text{Tl}(510.77 \text{ keV})$	$1\sigma$
$699 \pm 13$	$588 \pm 11$	$^{208}\text{Tl}(583.19 \text{ keV})$	$1\sigma$
$990 \pm 2$	$825 \pm 4$	$^{216}\text{Po}(804.9 \text{ keV})$ , the discrepancy probably comes from the Compton effect of the following peak, which we weren't able to fit	$6\sigma$
$1729 \pm 13$	$1430 \pm 11$	This peak is part of the one described in the analysis of the background, which hasn't been subtracted completely.	$3\sigma$
$2523 \pm 21$	$2080 \pm 18$	Single Escape Peak of the last peak. Its energy is 2056 keV	$2\sigma$
$3118.7 \pm 1.2$	$2567 \pm 8$	overlay of $^{208}\text{Tl}(2614.53 \text{ keV})$ and $^{212}\text{Po}(2610.0 \text{ keV})$	both $6\sigma$

Table 4: Results of the energy calculation from the channels.

#### 4.5. Angle distribution of the $^{22}\text{N}$ annihilation photons

We examined the angle correlation of the two 511 MeV photons with the  $^{22}\text{N}$  probe. As the background we measured 373 counts in 1000 s. Because the actual measurements are only 100 s long, we need to divide the count value by ten, resulting in 37 counts, since 37.3 counts doesn't make sense. The measured data minus the background is plotted in Figure 36. The counts have an error of  $\sqrt{n}$ , and for the angle we chose an read off error of  $0.5^\circ$ . On that data we fitted a Gaussian

$$\text{Gaus}(x) = a \exp\left(-\frac{1}{2} \left(\frac{x-b}{c}\right)^2\right) + d. \quad (4.7)$$

For the fit we calculated an  $\chi^2$  of 7.3. We calculated it with

$$\chi^2 = \sum \left(\frac{x-\mu}{\sigma}\right)^2. \quad (4.8)$$

We can see in Figure 36 that the amplitude is too big, which explains the relatively high  $\chi^2$ , but since we only care about the position of the peak and not its amplitude, it doesn't affect our results.

The factor  $b$  gives us the position of the peak. We get

$$\text{angle} = (-0.020 \pm 0.003)^\circ. \quad (4.9)$$

The error comes from the square root from the diagonal element from the covariance matrix and has nothing to do with the error on the counts or the read off error from the angle.

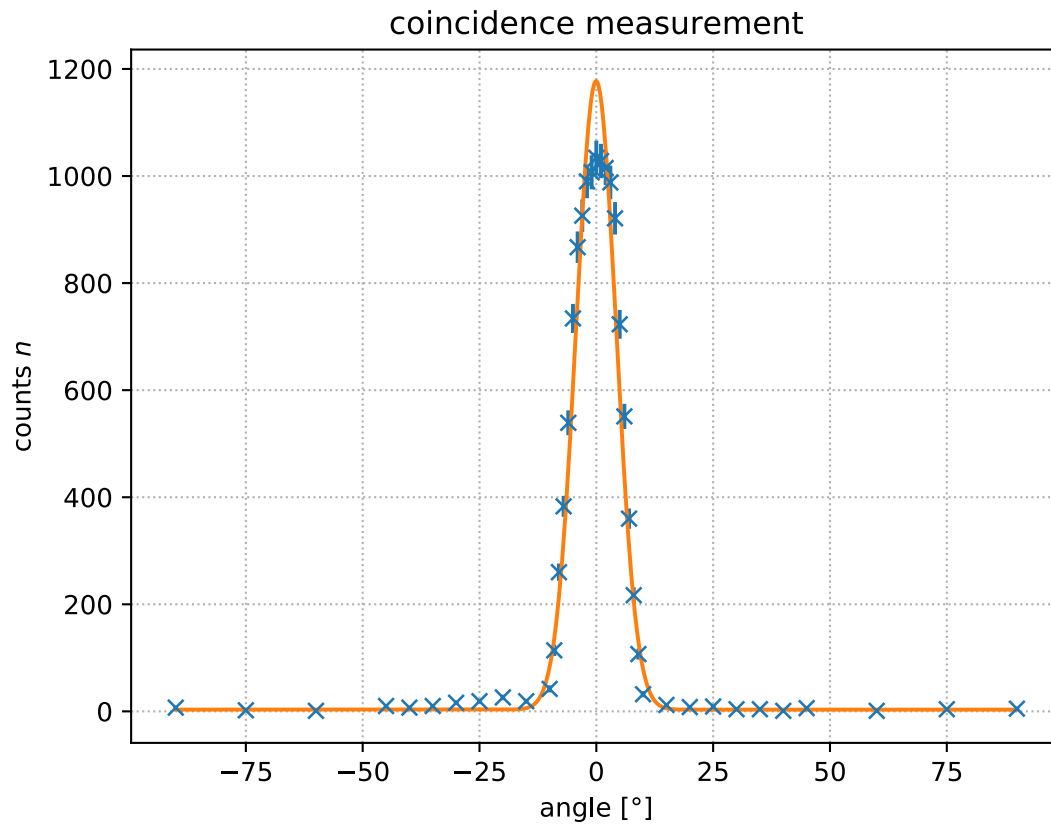


Figure 36: Coincidence measurement.

## 5. Summary and discussion

In the first part of the experiment we measured the spectrum of the background with an NaI scintillator. Here we were able to identify a peak with an energy of  $(1465 \pm 5)$  keV as belonging to the decay from the excited level of  $^{40}\text{Ar}$  to its ground level. The literature value for this decay is 1460.9 keV [1]. Furthermore we were able to determine a formula, that allows to transform the measured channels to energies. This we did by comparing the peaks in the spectra of  $^{22}\text{Na}$ ,  $^{152}\text{Eu}$  and  $^{60}\text{Co}$  to energies from literature. We were able to fit those data with the linear function

$$C(E) = (1.222 \pm 0.004) \text{ counts/keV} \cdot E - (19 \pm 2) \text{ counts}.$$

With this we were able to determine which peak in the spectrum of  $^{228}\text{Th}$  belongs to which transition. In some cases this worked well. In others there was quite a difference between our data and the theoretical values (see Table 4). We also realised, because the peak we found didn't subtract the corresponding one in this data completely, that our underground measurement and the measurement of the thorium spectrum don't fit completely, even though we didn't change any of the settings. This could also explain, why we didn't measure more peaks at the beginning of the spectrum. A possible way to enhance the spectrum would be to measure over a longer time period. This would give more counts so that the background wouldn't have as much effect on the results of the measurement. Another way to increase the result would have been to take overlaying peaks into account of the fit function.

In the second part of the experiment we did a coincidence measurement, to examine the angle distribution of two photons from a  $\beta^+$ . The measured data is shown in Figure 36. We measured, that the detector picks up the most photons at  $(-0.020 \pm 0.003)^\circ$ , meaning that the photons part at

$$(179.980 \pm 0.003)^\circ.$$

From the theory we expected  $0^\circ$  for the detector or  $180^\circ$  for the photons. With our value we are in a  $7\sigma$  range with that value. We have a relative error of 15 % on the angle for the detector. We have to keep in mind, that the error comes exclusively from the fit itself, and is not propagated from the read off error for the angle or from the error  $\sqrt{n}$  on the counts. With a relative high relative error and still a big sigma range to the expected value we conclude that there must be a offset of some kind. We suspect, that in the setup  $0^\circ$  isn't really  $0^\circ$ . With our data we can't really conclude whether the photons part in a  $180^\circ$  angle or not. But if we take the physical dimensions of our detector (especially it's width) into account, we would conclude, that they part at  $180^\circ$ , since the detector picks up photons not only for the set angle, but some degrees to the left and the right due to it's width.

## A. List of Figures

1.	Terms of the binding energy as function of the mass number $A$ .	4
2.	Proton and neutron core potential.	5
3.	Mass absorption coefficient for photons in lead.	8
4.	Decay scheme of $^{22}\text{Na}$ . Energies are in keV [1].	9
5.	Decay scheme of $^{60}\text{Co}$ . Energies are in keV [1].	9
6.	Decay scheme of $^{152}\text{Eu}$ . Energies are in keV [1].	10
7.	Decay row of $^{228}\text{Th}$ [1].	10
8.	Band structure in an inorganic scintillator [1].	11
9.	Scheme of a photo multiplier [1].	12
10.	Setup of the experiment [1].	13
11.	Block diagram for the measurement of the first part of the experiment [2].	13
12.	Block diagram for the measurement of the second part of the experiment [2].	14
13.	Negative signal from the preamplifier of the NaI detector.	15
14.	Signal from after the mainamplifier with $\tau = 0.5\ \mu\text{s}$ .	15
15.	Signal from after the mainamplifier with $\tau = 1\ \mu\text{s}$ .	16
16.	Signal from after the mainamplifier with $\tau = 2\ \mu\text{s}$ .	16
17.	Signal from after the mainamplifier with $\tau = 3\ \mu\text{s}$ .	16
18.	Signal from after the mainamplifier with $\tau = 6\ \mu\text{s}$ .	16
19.	Signal from after the mainamplifier with $\tau = 10\ \mu\text{s}$ .	16
20.	Bipolar signal from after the mainamplifier with $\tau = 1\ \mu\text{s}$ .	16
21.	Negative signal from the preamplifier of the organic detector.	17
22.	Bipolar signal from after the mainamplifier with $\tau = 0.5\ \mu\text{s}$ .	17
23.	Positive signal output from after the SCL.	17
24.	Negative signal output from after the SCL.	17
25.	Background data with fitted peak.	18
26.	Total sodium spectrum without background.	19
27.	Characteristic peaks in the sodium spectrum without background.	20
28.	Characteristic peaks in the europium spectrum without background.	21
29.	Characteristic peaks in the cobalt spectrum without background.	22
30.	Linear calibration of the MCA.	23
31.	Total thorium spectrum without background.	24
32.	Part one of the spectrum of Thorium without background.	25
33.	Part two of the spectrum of Thorium without background.	25
34.	Part three of the spectrum of Thorium without background.	26
35.	Part four of the spectrum of Thorium without background.	26
36.	Coincidence measurement.	28
37.	Our setup for the second experiment.	32
38.	Total europium spectrum.	32
39.	Total cobalt spectrum.	33
40.	Total thorium spectrum, logarithmic.	33

## B. List of Tables

1.	Peaks in the spectrum of sodium without background.	20
2.	Peaks in the spectrum of europium without background.	21
3.	Peaks in the spectrum of cobalt.	22
4.	Results of the energy calculation from the channels.	27

## C. References

- [1] T. Kotyk, *Versuche zur Radioaktivität im Physikalischen Fortgeschrittenen Praktikum an der Albert-Ludwigs-Universität Freiburg*, Staatsexamensarbeit, Physikalisches Institut, Fakultät für Mathematik und Physik, Albert-Ludwigs-Universität Freiburg
- [2] T. Klapdor-Kleingrothaus, *Versuchsanleitung Fortgeschrittenen Praktikum Szintillationsszähler*, Physikalisches Institut, Fakultät für Mathematik und Physik, Albert-Ludwigs-Universität Freiburg, 2017
- [3] W. Demtröder: *Experimentalphysik 4 - Kern-, Teilchen- und Astrophysik*, Springer-Verlag Berlin Heidelberg 2016
- [4] D. Meschede ed.: *Gerthsen Physik*, Springer-Verlag Berlin Heidelberg, 2015

## D. Appendix

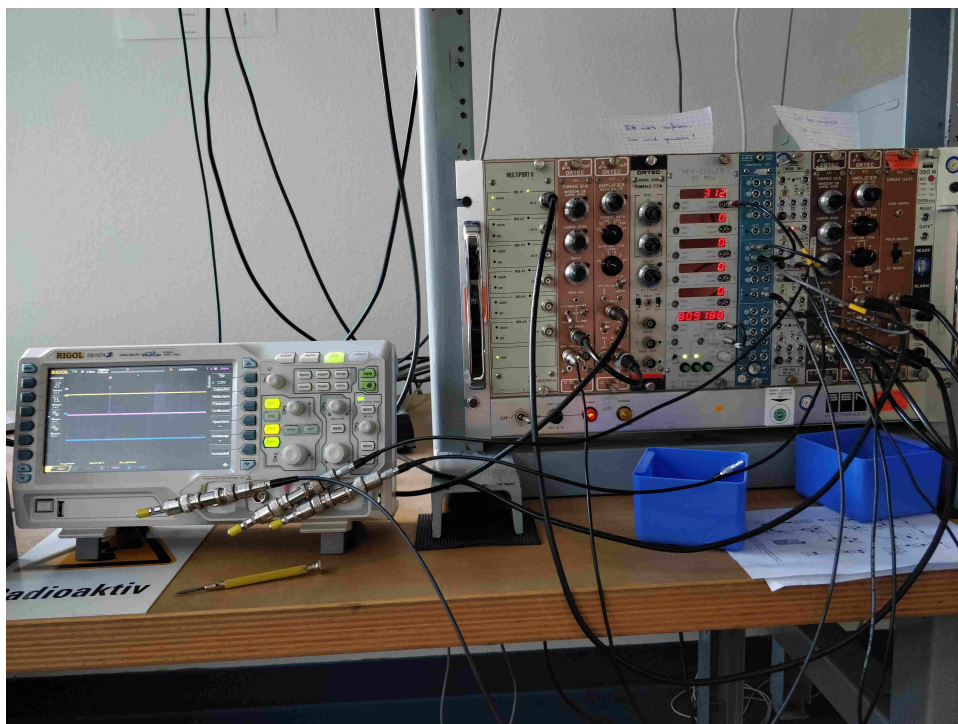


Figure 37: Our setup for the second experiment.

### D.1. Additional plots

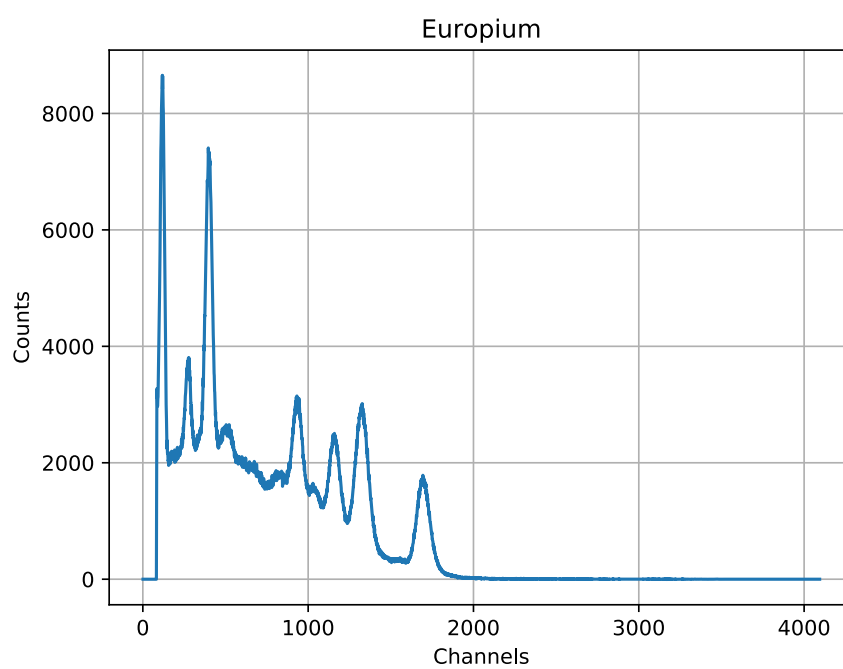


Figure 38: Total europium spectrum.



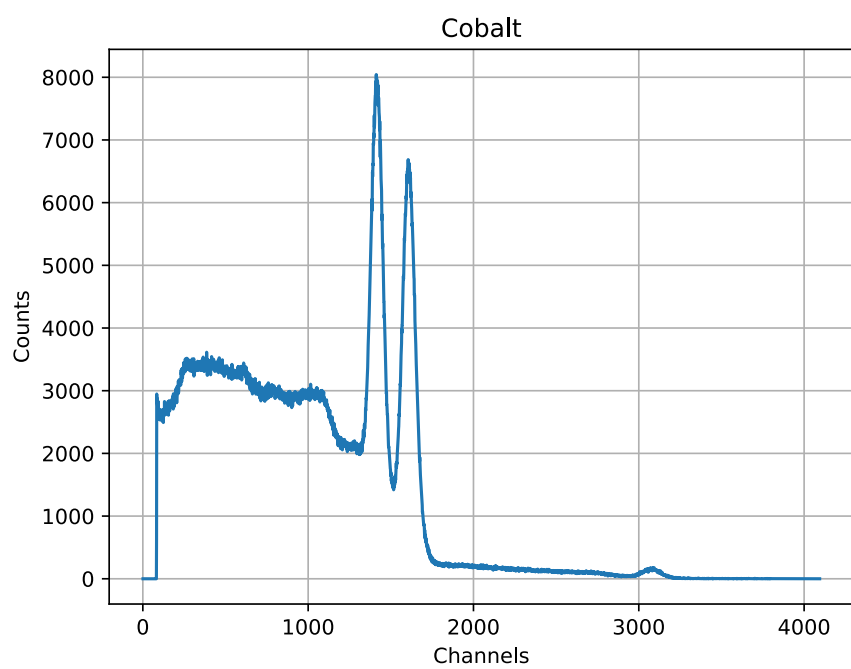


Figure 39: Total cobalt spectrum.

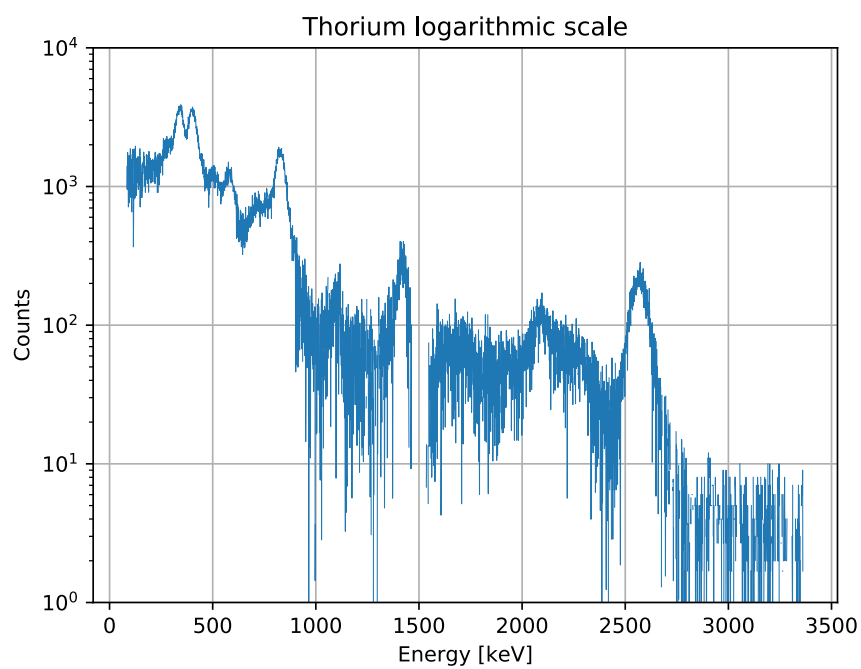


Figure 40: Total thorium spectrum, logarithmic.

## D.2. Original data

27.9.

### Sintaktion

Probe: Na

Ordner: New Folder 3

Datki: 1	Na, VV	
Signal negativ		
Datki: 2	Na, HV	shaping time: 2 $\mu$ s unipolar
3	Na, HV	shaping time: 0,5 $\mu$ s unipolar
4	Na, HV	shaping time: 1 $\mu$ s unipolar
5	Na, HV	shaping time: 3 $\mu$ s unipolar
6	Na, HV	shaping time: 6 $\mu$ s unipolar
7	Na, HV	shaping time: 10 $\mu$ s unipolar
8	Na, HV	shaping time: 7 $\mu$ s bipolar

*Handwritten scribbles*

Probe: Eu

Messzeit ca. 40 min

HV Amplifier gain: 6  
 Coarse gain: 20  
 shaping time: 3  $\mu$ s  
 BLR Antic  
 DELAY  
 NEG  
 UNI

Probe: Co

Messzeit ca. 30 min

Probe: Na

Messzeit ca. 30 min

### Koinzidenz Messung

Datki 9	Na, VV <sup>organ</sup>	
Datki 10	Na, HV <sup>organ</sup>	shaping time: 0,5 $\mu$ s
Datki 11	SCL <sup>organ</sup>	positiv
12	SCL <sup>organ</sup>	negativ

Datum 13

Timing Unit

Winkel	Counts	Messzeit 100s
80°	42	
75°	41	
60°	36	
45°	43	
40°	32	
35°	41	
30°	47	
25°	46	
20°	45	
15°	49	
10°	63	
9°	144	<del>±10</del>
8°	254	
7°	397	
6°	588	
5°	760	
4°	858	
3°	7025	
2°	<del>7000</del> 7052	
1°	1117	
0°	1077	
-1°	1044	
-2°	1027	
-3°	963	
-4°	904	
-5°	771	
-6°	576	
-7°	420	
-8°	297	
-9°	151	
-10°	79	
-15°	56	
-20°	63	
-25°	56	
-30°	53	
-35°	47	
-40°	44	
-45°	47	
-60°	33	
-75°	39	
-90°	44	

~~±10~~ ±0.5°

~~±10~~

Untergrund: Messzeit: 1000 s, counts: 373

Probe Th: ~~Los~~ ca. 75h

Unterschied: ca 3h